October 31, 1997

**Final Report**

**Title: System for Non-Destructive Testing of Tire Sidewalls**

**Contractor: EtaSYS, Inc.**
**2216 Liberty Dr.**
**Fort Collins, CO 80521**

**Contract number: N68335-97-C-0200**



**Key person: Justin Downs III**

---

## 1. Introduction

Tire inspection has previously used x-ray, shearography, and low-resolution ultrasound to inspect portions of a tire but not the entire tire [Dow97]. Recently Reis demonstrated acousto-ultrasonic inspection to detect belt damage in steel-belted radial tire sidewalls [Rei97]. Each technique is noted for its ability to detect certain types of problems within the rubber composite material of the tire in specific locations without providing a scan of the entire tire. Ultrasound in particular has been shown to be capable of detecting disbond and material property changes within the material [Rog92]. Specifically, the acoustic impedance of the material is altered in locations with disbond and/or material property changes. The change in acoustic impedance can be used to detect tire flaws using high-resolution 2-D scanning to locate areas with acoustic impedance changes.

Material property changes are often associated with heat damage to the material. Heat can cause additional crosslinking between long-chain molecules within material and change the acoustic properties. Heat can also cause a reduction in crosslinking known as reversion that also changes the acoustic properties of the material [Fre89]. Disbond affects the acoustic impedance of the material by reflecting a part of the ultrasound beam.

Recent advances in data-acquisition and control technology have allowed large data-set, high-speed inspection systems to be produced. The use of inexpensive PC (Personal Computer) based data-acquisition, control, signal-processing and display enables a cost-effective tire scanning system. Before developing a complex inspection system for aircraft tires, the ability to detect material property changes in aircraft tires is demonstrated.

2216 Liberty Dr.
Fort Collins, CO 80521

January 8, 1998

Defense Technical Information Center (DTIC)
Attn: DTIC-OC
Cameron Station, VA 22304-6145

To Whom It May Concern:

EtaSYS recently completed U.S. Navy Phase I SBIR #N68335-97-C-0200. In accordance with contract clause H.6 and DFAR 252.235-7011, I am forwarding to you two copies of the final report for this SBIR contract.

Please contact me if there are further questions. Thank you very much.

Sincerely,

Justin Downs III

Chief Engineer
EtaSYS, Inc.
970-493-7165

## 2. Transducer operating conditions.

For a tire scanner to detects small defects, the resolution of the transducer is critical. Transducer resolution is characterized by the size of the region of maximum acoustic pressure in a cross-sectional slice along the central axis. A number of factors determine the size of the region known as the 'spot size'. Piezoelectric ultrasonic transducers are available in a large variety of operating frequencies, sizes, focusing capabilities, and wave generation types. In addition, limitations are imposed on transducer operating conditions by the inspection to be performed. Figure 2.1 shows a simple diagram of a circular flat transducer to be used for tire inspection.

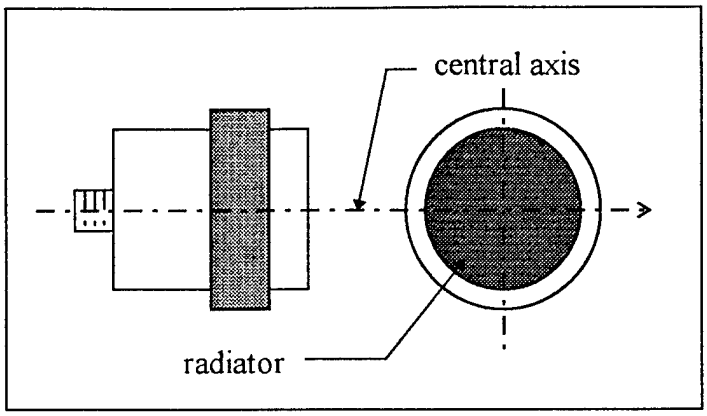


**Figure 2.1: Circular flat transducer.**

### 2.1 Transducer operation.

Ultrasonic transducers for this type of inspection are constructed to operate at particular frequencies. Transducers operate by electrically exciting an active element, typically made of piezo-electric or ferro-magnetic material. Applying an electric potential to opposite sides of a piezo element causes contraction of the material along a selected axis followed by expansion when the charge is removed [Kra83]. Careful selection of the excitation axis can generate longitudinal (compression) or transverse (shear) sound waves to be radiated by the transducer. For tire inspection by relative attenuation, only longitudinal waves are important. The frequency of the transducer is characterized by the resonant mode of the active element. When excited, a range of frequencies are generated and radiated. The frequency with maximum power in the range is referred to as the "center frequency" of the transducer [Pan95].

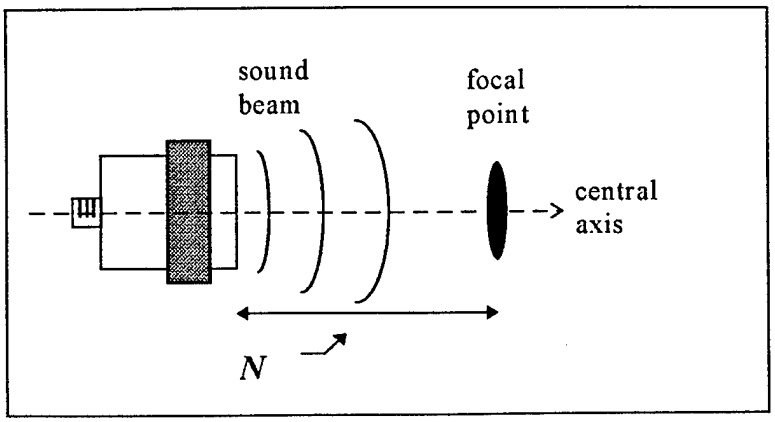

Figure 2.2: Near Field Distance.

Transducer sound field physics are similar to that for optical light fields. The sound beam can be focused, refracted, or reflected. Diffraction phenomena occur that cause an interference structure defined by Huygens' principle. For emission from a flat circular radiator, interference in front of the radiator causes a series of maxima and minima in the sound pressure along the central axis of the transducer [Kra83]. The location of the last maxima at a distance $N$ from the face of the transducer is known as the near field distance and is the natural focus of the transducer shown in Figure 2.2. The location of the maxima and minima can be calculated by [Kra83]:

:

$$p = \left| p_o \, 2 \sin\left( \frac{\pi}{\lambda} \left\langle \sqrt{\frac{D^2}{4} + a^2} - a \right\rangle \right) \right| \qquad (2.1)$$

where:

$p_0$ = *initial acoustic pressure, (usually* $p_0 = 1$*)*
$\lambda$ = *wavelength*
$D$ = *diameter of radiator*
$a$ = *distance along central axis*

An example of this is shown in Figure 2.3. The transducer face is taken to be at position 0 at the origin of the graph. A series of maxima and minima occur moving away from

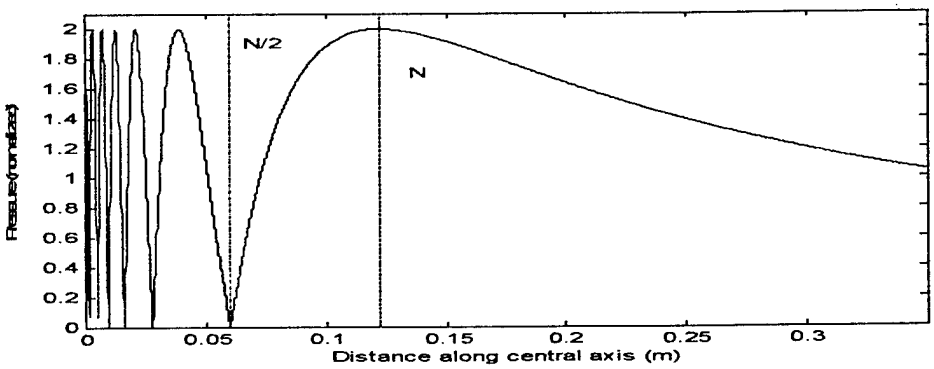


**Figure 2.3: Acoustic pressure along central axis, flat transducer.**

axis due to interference effects until a final maximum is reached at **N**. The point **N** determines the near field distance and is the natural focal point of the transducer. The distance **N** can be calculated by [Kra83]:

$$N = \frac{D^2 - \lambda^2}{4\lambda} \qquad (2.2)$$

Transducers are often focused spherically or cylindrically to increase the acoustic pressure along the central axis around the focal point. Focusing also assists in reducing cross-sectional area of the region of maximum pressure (or 'spot size'). The focusing is accomplished by using curved radiators or a contact lens in front of a flat radiator. The contact lens is constructed of a material with suitable acoustic impedance properties to match the active element and transmission medium as closely as possible. For a focused transducer, the regions of maximum sound pressure in front of the transducer are given by [Kra83]:

$$p = p_0 \left| \frac{2}{1 - \frac{a}{r}} \right| \left| \sin\left[ \frac{\pi}{\lambda} \left( \sqrt{(a-h)^2 + \frac{D^2}{4}} - a \right) \right] \right| \qquad (2.3.1)$$

$$h = r - \sqrt{r^2 - \frac{D^2}{4}} \qquad (2.3.2)$$

where: $r$ = *radius of curvature of the radiator.*

Figure 2.4 shows an example of how focusing affects the near field and maximum power of the acoustic beam. Figure 2.4A shows the sound pressure moving away from the

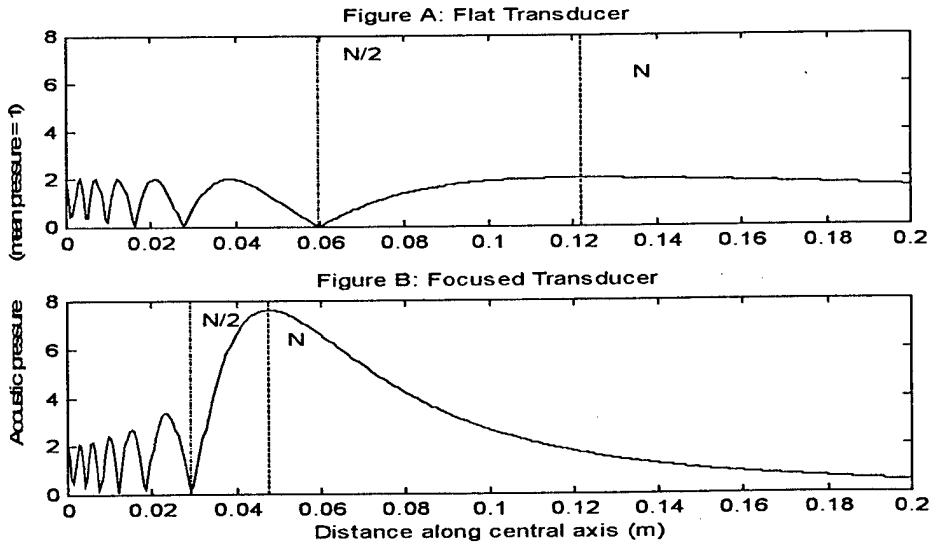


Figure 2.4: Maximum sound pressure along central axis; flat vs. focused transducer.

radiator face for a 1.5" diameter flat transducer operating at 0.5 MHz and is equivalent to that shown in Figure 2.3. The maximum sound pressure is 2 times the mean pressure. Figure 2.4B shows the sound pressure along the central axis for a similar transducer focused at 2.25". The focused transducer exhibits maximum sound pressure almost 8 times the mean enhancing the ability of the transducer to insonify a small inspection zone. Conversely, a focused transducer operated as a receiver will have 8 times the sensitivity of a comparable flat transducer. There are tradeoffs associated with focusing. Comparison of Figures 2.5 A and B clearly show that the location of the near field is shifted closer to the radiator face. In addition, the length of the maximum pressure field is shortened. The length of the maximum pressure field is known as the 'focal zone' and is often a critical element in transducer selection. The interference fringe generated in the near field classically prohibits its use for effective measurements and most measurements will be made using the far field after the *N/2* point [Kra83].

It is important, for the proposed tire inspection, to know the location of the focal zone accurately. The focal zone is located where the acoustic pressure drops by -6dB along the central axis with the length determined by [Pan95]:

$$F_z = NS_F^2\left[\frac{2}{(1+0.5S_F)}\right] \qquad (2.4)$$

where:

$F_z$ = *length of focal zone*
$N$ = *near field distance from Eq. 2.4*
$S_F$ = *normalized focal length* = $\frac{focallength}{N}$

With focused transducers, the beginning and end of the focal zone usually must be determined iteratively using Eqs. 2.5.1,2 [Kra83]. The long wavelengths involved combine with the small relative aperture of a transducer to provide long focal zones. The long length of the focal zone for this application is critical for high-speed inspection to be possible. This will be examined in Section 2.4.

The operating conditions of a transducer determine the resolution for a particular transducer. The spot size for a transducer is the maximum beam diameter in a cross-sectional slice along the central axis where the acoustic pressure has not been attenuated more than -6dB. Figure 2.6 shows an illustration of this.

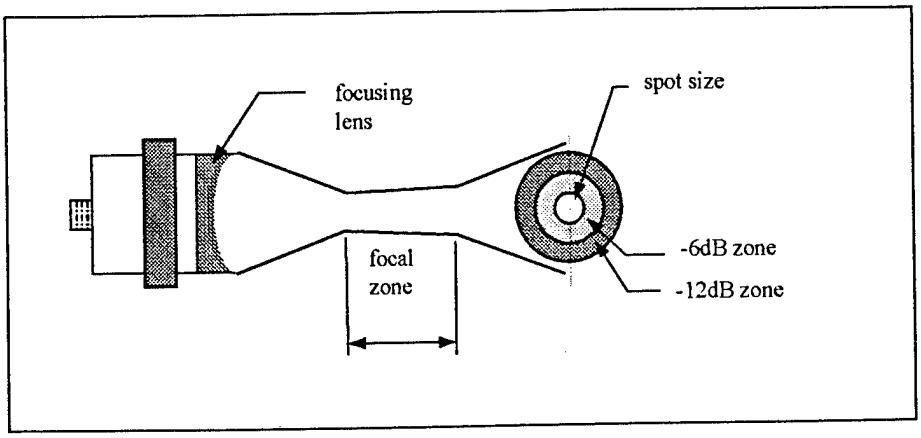


**Figure 2.5: Focused transducer spot size.**

In general, the spot size of a focused transducer can be estimated by [Pan93]:

$$BD_{(-6dB)} = \frac{1.028Fc}{fD} \qquad (2.7)$$

where:

$BD$ = *beam diameter*
$F$ = *focal length*
$f$ = *frequency*
$c$ = *sound velocity in transmission medium*
$D$ = *diameter of transducer*

The beam field pattern moving away from the central axis is also a series of maxima and minima arranged in concentric rings and can be calculated for a focused transducer with a simple model where [Kra83]:

$$p_t = \left| p_{\max} \frac{2J_1(x)}{x} \right| \qquad (2.8.1)$$

$$x = \frac{\pi D q}{\lambda} \qquad (2.8.2)$$

where:

$p_t$ = *pressure transverse to the central axis*
$p_{max}$ = *maximum sound pressure at axis from Eqs. 2.5.1,2*
$q$ = *distance at right angles to the central axis*
$J_1$ = *first order Bessel function*

This relationship that describes the point spread function (PSF) of a transducer. An understanding of the PSF for the transducer is critical to use deconvolution of the PSF to enhance the resolution of a system [Dow96].

## 2.2 Transducer limitations.

Sections 2.3.1 and 2.3.2 contain a partial description of the nature of the acoustic field generated by an ultrasonic transducer; relationships inherent in sound beam physics. For

imaging, the acoustic field must display sufficient resolution to detect critical defects in the tire.

Center frequency requirements.

Rogers [Rog92] has shown that tires can be inspected for disbond and some material property changes using ultrasound through transmission techniques. Disbond and material property changes produce attenuation of the ultrasound beam from reflection at disbonds and changes in material damping that result from altered structure. Tire inspection can then be performed by comparing the relative attenuation of an elastic wave that propagates through the tire at different points around the tire. However, to provide high spatial resolution inspection, a large number of points need to be inspected and compared.

When Rogers [Rog92] inspected truck tires at a frequency of 0.5 MHz, the low frequency was selected to prevent detection of the steel belts. The high acoustic impedance mismatch between rubber and steel belts attenuated the ultrasound signal at higher frequencies due to reflection at the belts. The steel belts are easily detected at higher frequencies.

Aircraft tires are typically constructed using nylon belts with an acoustic impedance very close to that of the surrounding rubber matrix [Kra83]. The similar impedance allows far higher resolution scanning of the rubber matrix without interference from steel belts. A disbond occurring at a belt separation or cord break will be easily detectable by its relative attenuation compared with surrounding good material. Nylon belts in aircraft tires are typically constructed of cord with a diameter approximately 1/32". Characterizing defects in the rubber composite including belt failure and separation requires a spot size capable of detecting flaws as small as 1/32.

## 2.3 Transducer size.

In a through transmission inspection for tires, it will be necessary to place one transducer within the tire. Sections 2.3.1 and 2.2.2 discuss some of the tradeoffs inherent in transducer design and selection for an inspection. Eq. 2.7 shows that for a fixed transducer frequency, the spot size can be altered by varying either the size of the transducer or the focal length. The focal zone of the transducer is important since it sets the proximity of the transducer relative to the tire wall. If the focal zone is long with a close focal point, the transducer need not be a consistent distance from the tire to maintain accurate resolution. Since standard transducer casings are directly related to radiator face size, a limit is imposed by whether a transducer will fit inside a tire casing. In addition to smaller spot size, larger radiators also have greater focal zones. For this inspection the largest transducer that will fit into the tire is 1". The length of a 1" transducer with wiring harness is about 3.5". The width at the bead, (see Figure ??) of the small aircraft tire needing inspection is about 2". This effectively sets an upper limit on how large a transducer may be selected for inspection.

2.4 Focal zone requirements.

For maximum efficiency during setup and inspection, it would be satisfactory to inspect the sidewall and crown region without needing complex motion of the transducer to conform to the tire profile. By selecting a transducer with a large focal zone, the transducer motion can be a simple as a straight line. Figure 2.6 shows an example where

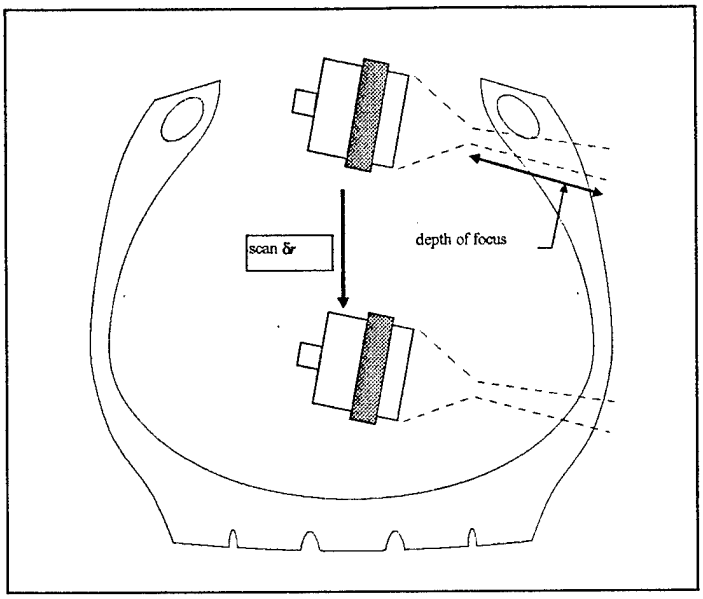


**Figure 2.6: Depth of focus and transducer motion.**

the sidewall of a tire can be inspected with simple straight line motion by utilizing the large depth of focus of the transducer.

2.5 Spot size and focal zone calculations.

A spot size of at least 1/16" is desired to provide adequate resolution for tire inspection. The spot size can be estimated using Eq. 2.7 and it is evident that a number of factors influence the spot size. While the focal length is a factor, the spot size is primarily governed by the center frequency and the diameter of the radiator. Aircraft tires are produced in a wide range of sizes. Smaller tires will prevent a large transducer from being admitted inside the tire for a through transmission inspection. If the transducer is restricted to a 1" radiator face to be small enough to enter a small tire, the factors governing the spot size are primarily the center frequency with some input from focal length.

Some aircraft tires are small enough that the transducer itself will not fit inside the tire horizontally to perform an inspection as shown in Figure 2.6. To perform an inspection on the inside of a tire, a special low-profile transducer or transducer with reflector may have to be used. Figure 2.7 shows an example of a transducer and reflector.

3. Experimental inspection.

Section 2 provided a theoretical basis for transducer operating conditions. Rogers and Downs [Rog92][Dow97] achieved good results inspecting steel belted radial tires by through transmission ultrasound inspection. However, aircraft tires have not been inspected by through transmission ultrasound before this study. Steel belted radial truck tires have a far less complex structure in the sidewalls than a nylon belted bias ply aircraft tire. In addition, to achieve higher resolution for aircraft tire inspection, higher frequency ultrasound needed to be used than that used by Rogers and Downs. In general, higher frequencies will tend to be attenuated more in an elastic medium than lower frequencies. Before this study, it was unknown if the attenuation properties in the complex aircraft tire structure would permit through transmission inspection.

To determine if the attenuation properties of the tire sidewall would permit inspection by ultrasound, a tire needed to be point tested for ultrasound transmission and then xy scanned for comparison of adjacent areas. In point testing, a single spot is selected on the tire sidewall and an ultrasound pulse directed at the spot with a receiver on the opposite side of the tire. The pulse signature after transmission is recorded for analysis. In xy scanning, a large number of points are inspected at regular intervals and the relative attenuation properties of the material are built up into an image of the tire.

Total immersion in a water tank is used to reduce energy loss due to reflection of the sound beam at interfaces. The acoustic impedance of water is close to that of rubber and nylon promoting low energy losses at the water/rubber interface. Acoustic impedence is defined as [Kra83]:

$$\rho c = Z$$

where:

$\rho$ = density ($kg/m^3$)
$c$ = sound velocity in material (m/s)
$Z$ = acoustic impedence ($kg/m^2s$)

The acoustic impedence is a measure of how easily sound travels through the material. Large impedence mismatches will cause reflection at the interfaces between materials. Acoustic impedences ($10^6 kg/m^2s$) for the materials are [Kra83]:

$H_20$ = 1.5
rubber = 1.4 - 2.8
nylon = 2.4 – 3.1

3.1 Experimental setup.

Previous equipment had been constructed to automate truck tire inspection [Dow97]. However, the small size of aircraft tires prohibited the sensor heads of the previous system from being used as a test bed for aircraft tire inspection. To overcome this difficulty, a piece of aircraft tire, shown in Figure 3.1, was removed from a tire to be used for simple

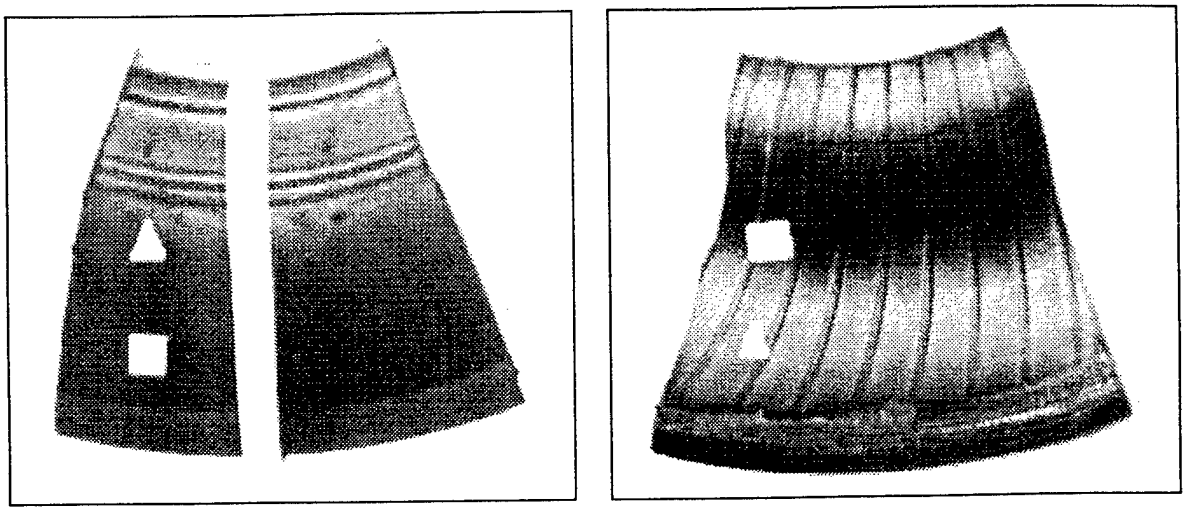

**Figure 3.1: Tire section showing foam tape attached, (outside-inside).**

point and x-y scanning. A device to hold two transducers on opposite sides of the tire was constructed as shown in Figure 3.2. The device holds a circular flat transmitting

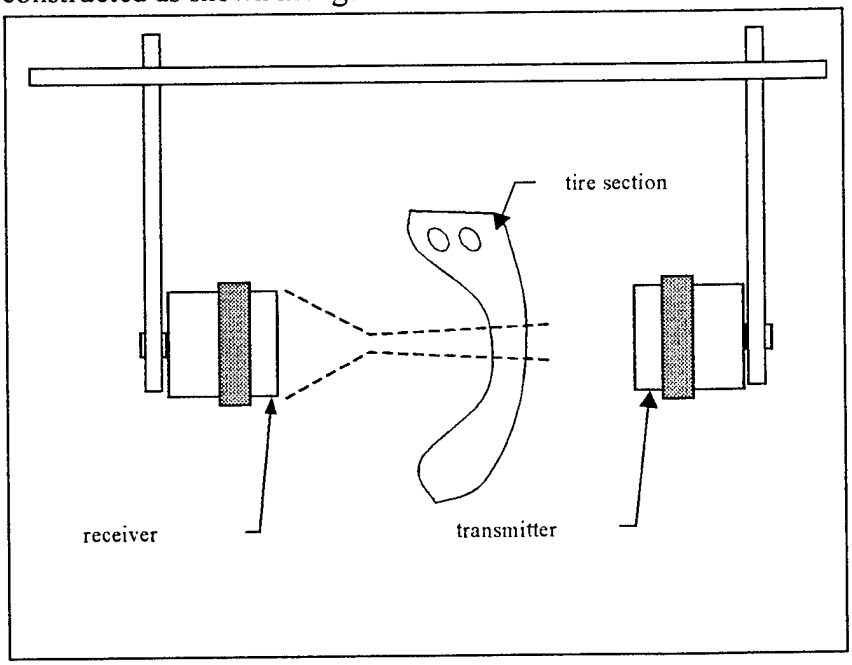


**Figure 3.2: Transducer setup.**

transducer on the outside of the tire, and a spherically focused receiver on the inside. Figure 3.3 shows an image of the transducer setup in the inspection tank with transducers and the tire section. The sensing head shown in Figures 3.2 and 3.3 was connected to a

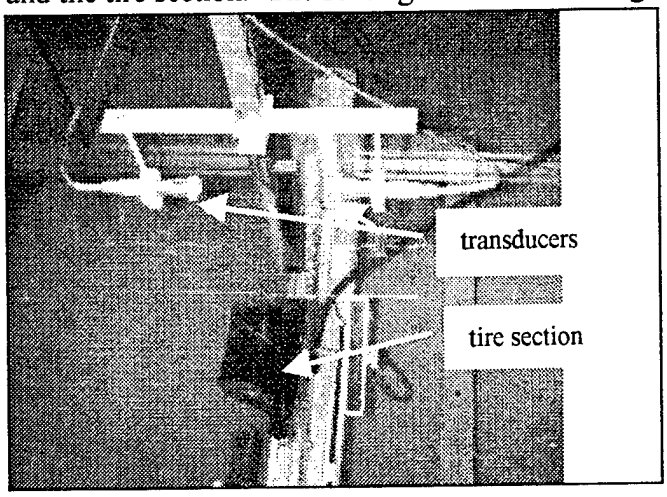


**Figure 3.3: Transducers in tank with tire section.**

Panametrics Model 5072PR pulser/receiver and the output sent to a Tektronix THS 710 oscilloscope.

3.2 Point testing.

For total tire inspection, it was necessary to show that the acoustic pulse could be directed through the tire and a meaningful return received on the other side (called an a-scan). Several locations on the tire were selected as representative by direct observation of the acoustic pulse signature at the location. A location near the bead and one near the

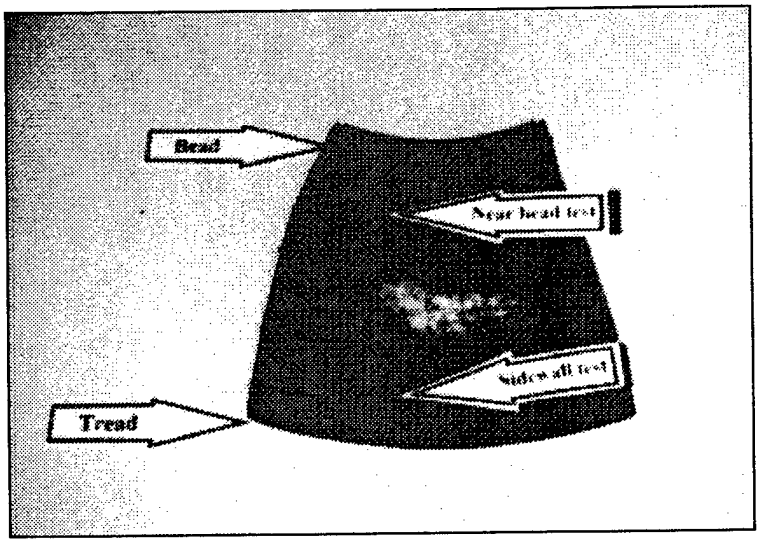


**Figure 3.4: Point testing locations.**

sidewall were selected for point testing and comparison, shown in Figure 3.4. The tire

construction near the bead is thicker and more complex than that near the sidewall necessitating independent measurements being performed at different locations.

For comparison purposes, ultrasound frequencies of 0.5 MHz and 2.25 MHz were used in the through transmission point testing. Transducers for each frequency were mounted and aligned in the sensor head. An open water scan was recorded to compare with through transmission scans. A scan was then performed at the sidewall location followed by a scan at the bead location. Gain was applied to the output of the receivers until the signal display reached similar levels for comparison. Figure 3.5 summarizes the results of the scans.

Figure 3.5A shows a 0.5 MHz scan through open water with 5 dB gain applied to the output of the receiving transducer. Figure 3.5C shows a through transmission signal, gain of 25 dB with the 0.5 MHz transducer at the sidewall location shown in Figure 3.4. Figure 3.5E shows the 0.5 MHz transducer and gain of 45 dB at the bead location shown in Figure 3.4.

Figure 3.5B shows a 2.25 MHz scan through open water with 5 dB gain applied to the output of the receiving transducer. Figure 3.5D shows a 2.25 MHz through transmission signal, gain of 40 dB at the sidewall location. Finally, Figure 3.5F shows the 2.25 MHz signal with gain 55 dB at the bead location.

## 3.3 XY scanning

XY scanning takes a large number of point scans and builds them into an image (called a c-scan). The experimental sensor head was connected to an xy motion table to step the transducer head over the surface of the tire section. A gated peak detector, Matec PD2000, was used to determine the peak voltage received at each point inspected. Output of the peak detector was directed to a MicroStar DAP 1200e data acquisition board and the peak voltage was recorded at each step. An image was built up using the peak voltages detected by the system for each pixel value. The experimental setup is diagramed in Figure 3.6.

To determine if the system was capable of resolving differences in attenuation, artificial flaws were attached to the tire section. Artificial flaws needed only to change the attenuation properties of the material and any material with air gaps enclosed in it will provide this. Foam tape was applied as shown in Figure 3.1 to simulate attenuation changes. The foam tape was applied on the inside and outside of the tire in several patterns to attempt recovery of the shape. Scans of 56x92 steps were performed with a step size of 1/16".

Figure 3.7 shows a series of images from scanning the tire section using 0.5 MHz and 2.25 MHz ultrasound. In 3.7A, the tire was scanned at 0.5 MHz. Initially the gain on the receiving transducer was set to 35 dB. However, during the scan it soon became evident

that the gain was too high as the scanner moved away from the bead. The high gain clipped the received signal and reduced the resolution until the gain was reduced to 25 dB at step 43. The central strip of foam tape is visible but resolution is marginal. The larger spot size of the 0.5 MHz transducer prohibits detecting the smaller foam flaws. Figure

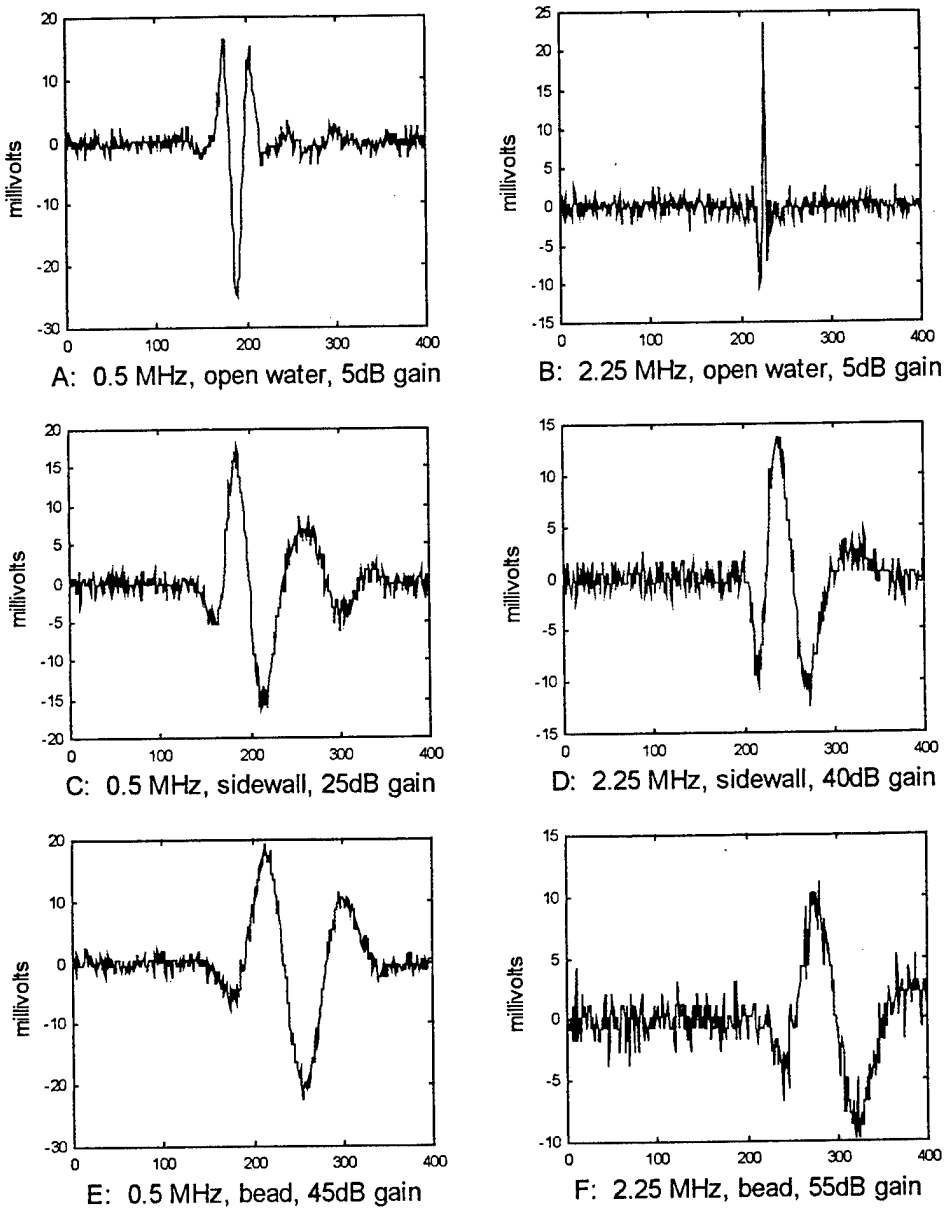


**Figure 3.5: Ultrasonic signal transmission.**

3.7B shows the tire section inspected at 2.25 MHz. The central stripe of foam tape is clearly visible. On each side of the central stripe, smaller flaws simulated with tape shown

in Figure 3.1 are also visible. Constant gain across the entire scan prevents higher resolution since the gain needed near the bead is far higher than the gain needed in the relatively transparent sidewall.

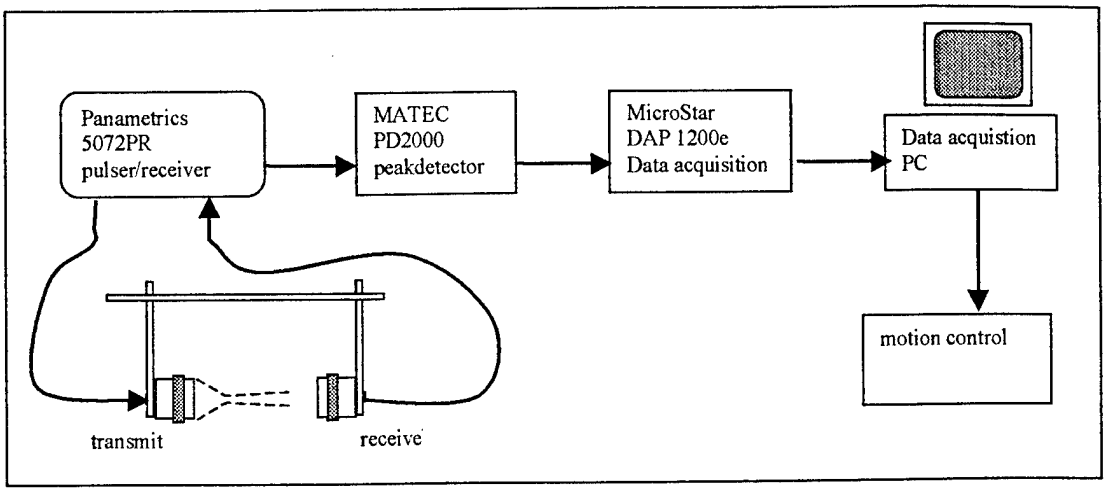


**Figure 3.6: Scanning diagram.**

Figure 3.7A

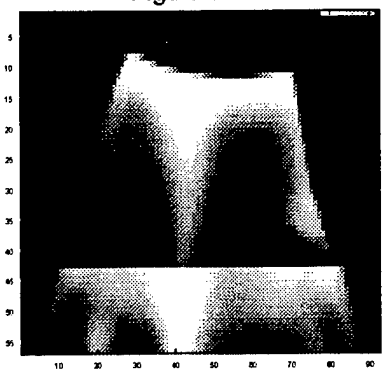

0.5 MHz, Gain 35/25 dB, straight through

Figure 3.7B

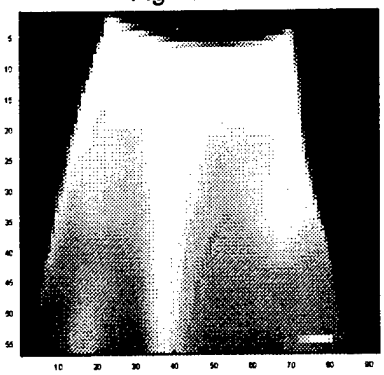

2.25 MHz, Gain 35 dB, straight through

Figure 3.7C

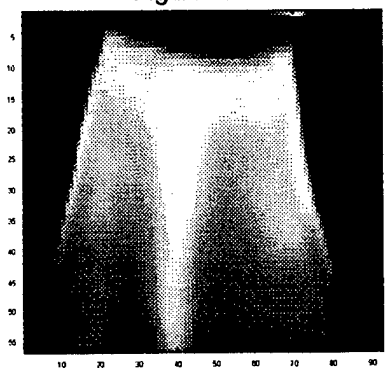

2.25 MHz, Gain 45 dB, 90 deg reflector

Figure 3.7D

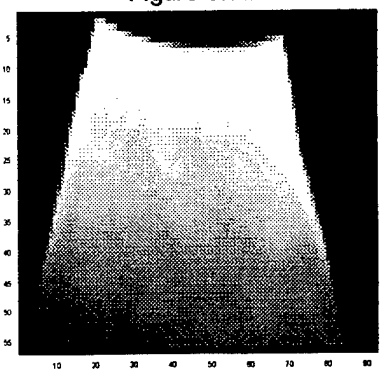

2.25 MHz, Gain 35 dB, straight, no flaw s

**Figure 3.7: Ultrasound images.**

Figure 3.7C shows the same section inspected with a 90° reflector attached to the transducer. The purpose of the reflector was to determine if the inspection could be made in the event that the transducer must be held vertical inside the small tire. Figure 3.7D shows the tire section inspected without foam tape attached. In 3.7D, the tire cross plies are easily discernable (The low resolution printout reproduced for this document does not display flaw characteristics nearly as well as the much higher resolution computer monitor used for data display. On the computer monitor display, far greater detail is available.).

## 3.4 Circumferential scanning.

Section 3.3 showed that ultrasound signal attenuation changes could be detected easily in the tire material. Full tire scans of the tire were necessary to determine if the results can be extended to the entire tire. Scanning the tire, as originally envisioned, was to be performed by using an array of paintbrush transmitters arranged around the outside of the tire in a manner to fully insonify a profile section of tire as shown in Figure 3.8. A

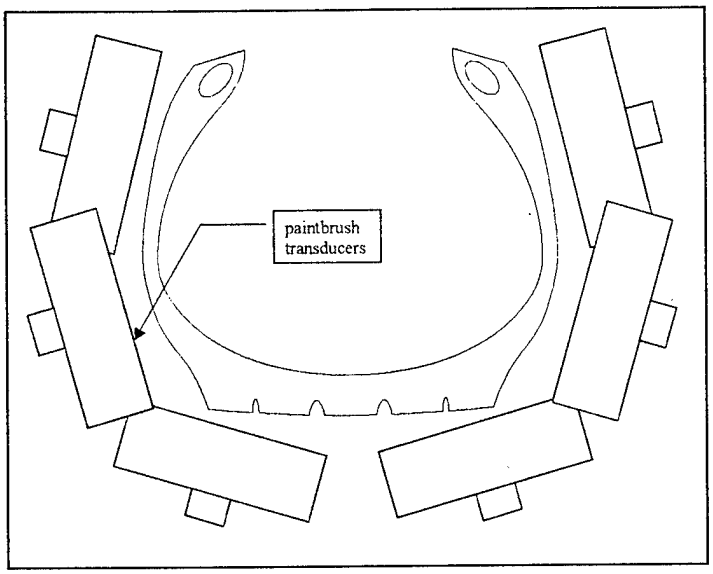


**Figure 3.8: Tire profile with paintbrush transducers.**

receiver was then to be placed inside the tire aligned with each paintbrush. The small size of the tire prevented standard transducers from being inserted into the tire. However, standard transducers can be placed vertically inside the tire. Instead of direct alignment of the central axis, acoustic mirrors would be used to align the central axis of the receiver with each paintbrush. This was investigated in Section 3.3. A mount was constructed for this purpose and tested. During initial testing, the paintbrush transducers proved to be unable to supply sufficient energy for the signal to pass through the tire without severe attenuation. Typical output of the receiving transducer with 55 dB amplification was less than 5 mV. In this range, noise in the receiving system became a significant portion of the signal.

To overcome the failure of the paintbrush concept, a series of mounts were constructed, shown in Figures 3.9-11, to hold a pair of circular transducers along a central axis and perform individual scans of sections of the tire. The mounts were designed to inspect

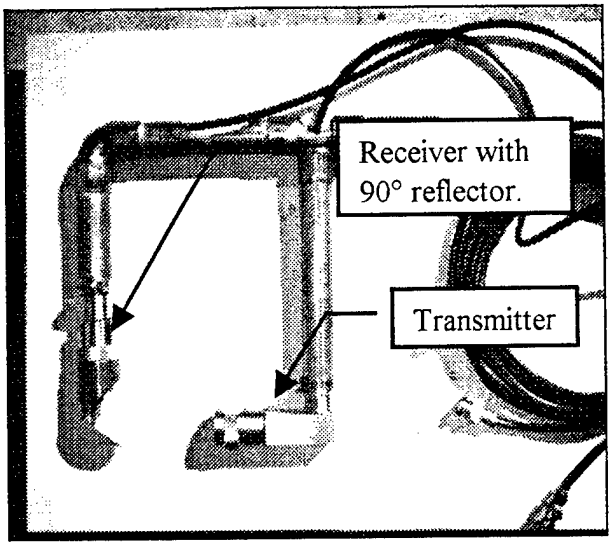


**Figure 3.9: Sidewall inspection fixture.**

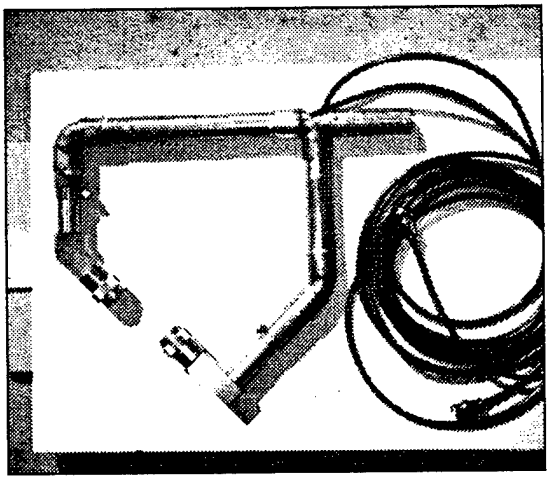

**Figure 3.10: Shoulder inspection fixture.**

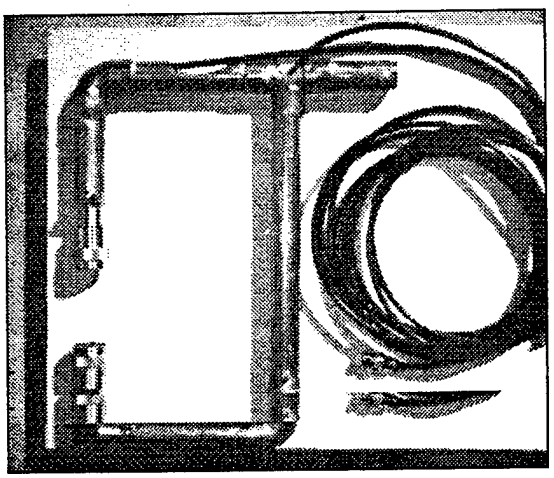

**Figure 3.11: Crown inspection fixture.**

individual portions of the tire circumfrentially as shown in Figure 3.12. The individual scans would later be combined into a single map of the tire. For the purposes of this study, the fixtures were not optimized and could not inspect the tire fully. However, points of interest were identified and it is shown that inspection is possible over the entire tire. Full tire inspection could be made possible by development of a dedicated motion system to move a transducer pair over the entire profile.

A complete tire was mounted on the tank and foam tape flaws applied to simulate material attenuation flaws (shown in Figure 3.13). In Figure 3.13, two strips are applied followed by a series of squares. The strips are ½" wide and end 1" before the bead. The large

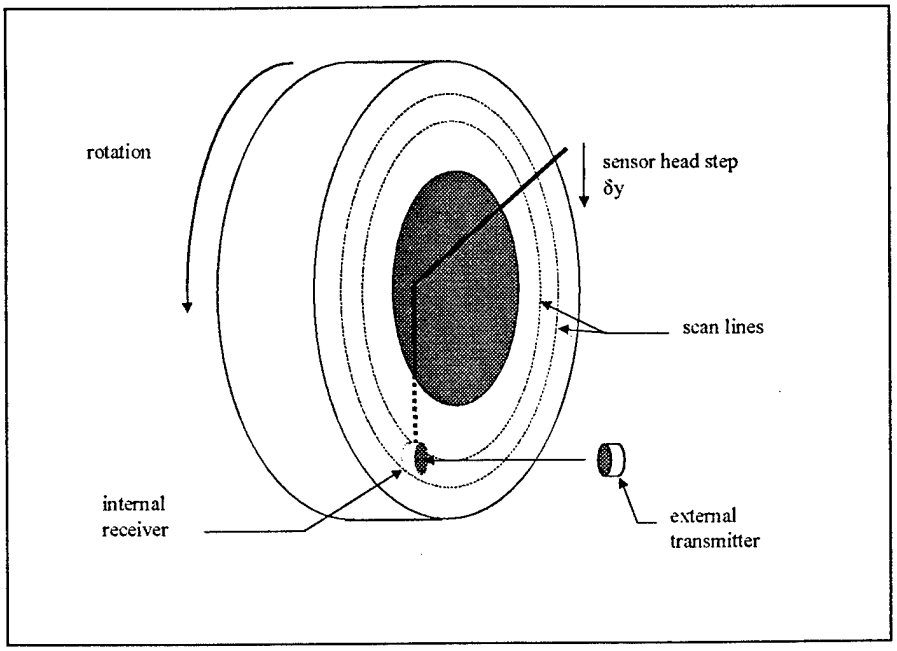


**Figure 3.12: Circumferential scanning.**

squares are 1" and the small ½" on a side. Approximately 120° clockwise from the double strips is a second foam strip. Located near the bottom of the picture is a fourth strip that was masking tape applied to simulated a very low attenuation change. The strips are used

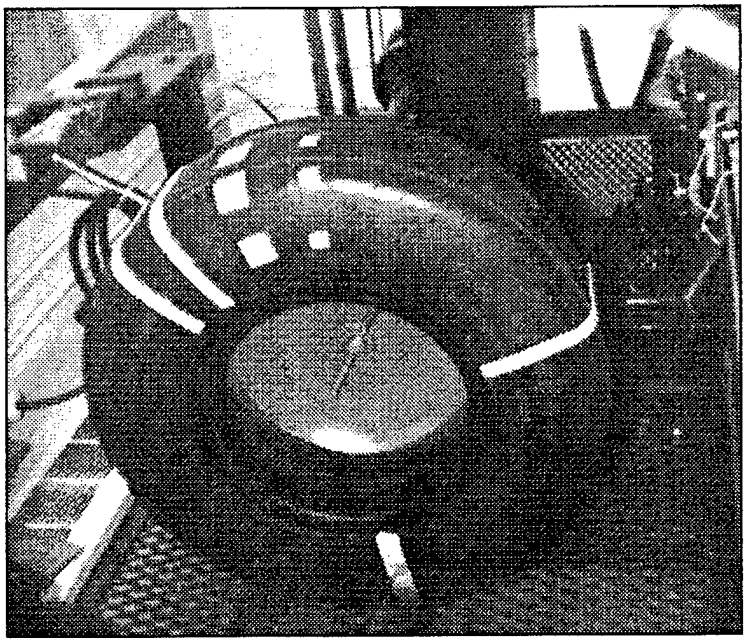

**Figure 3.13: Mounted tire with simulated flaws.**

to determine if the tire can be inspected bead to bead and the squares are used to check resolution of the inspection in the sidewall, crown, and critical shoulder regions.

If a line is drawn on the tire profile from one bead to the other, as the strips shown above, the thickness of the tire varies greatly along the line. In the thicker portions, more gain needs to be applied to the receivers for a meaningful signal to be received. However, if the same gain that is applied to the thick, highly attenuative bead region is applied to the thinner sidewall, clipping in the amplifiers can occur with an associated loss of attenuation information. Conversely, if the lower gain needed in the sidewall region is applied at the bead region, the received signal is small and might possibly mimic flaws in a good region.

It is desirable to have a relatively constant output of the receiving amplifiers for comparison with the attenuation properties of adjacent areas. During scanning, gain applied to the receiver output was adjusted after each scan revolution to account for variation in the natural properties of the tire as the receiver was stepped across the profile. An average 300 mV level output was used as a baseline. In general, gain applied to the receivers at the bead was 55 dB and was lowered in steps across the sidewall to 35 dB at the shoulder. Gain across the crown was held at a constant 30 dB. Flawed areas are identified as areas where the receiver output amplitude is not as great as adjacent areas.

To provide a better highlight of the flaw map, the data was modified by the algorithm:

$$\mathbf{M} = \left| \left[ \frac{\left(M_{original} - m_{\min}\right)}{\left(m_{\max} - m_{\min}\right)} * 255 \right] - 255 \right| \qquad (3.1)$$

where:

| | |
|---|---|
| **M** | = processed image |
| $M_{original}$ | = original scan |
| $m_{min}$ | = minimum of original scan |
| $m_{max}$ | = maximum of original scan |

**M** is then a map of the data expanded into range of 0 to 255. In addition, the high recorded measurements are converted to lows and lows to highs so flaws will be displayed as contrasting areas. To further highlight the flaws, a non-linear scaling is applied where:

$$p' = \frac{p^4}{5x10^7} \qquad (3.1)$$

where:

| | |
|---|---|
| $p'$ | = new pixel value |
| $p$ | = old pixel value |

and $5x10^7$ is a scaling parameter to prevent over-ranging 255 maximum value.

The circumferential scans were performed at 1/16" resolution (step size of the receiving transducer). Figure 3.14 shows the bead, sidewall, and crown scans combined into one image that covers approximately one-half the tire. The image has been enhanced by the algorithm in Eqs. 3.1,2. Only one half was inspected due to the complexity with inspection by three inspection fixtures. The simple inspection fixtures did not allow a

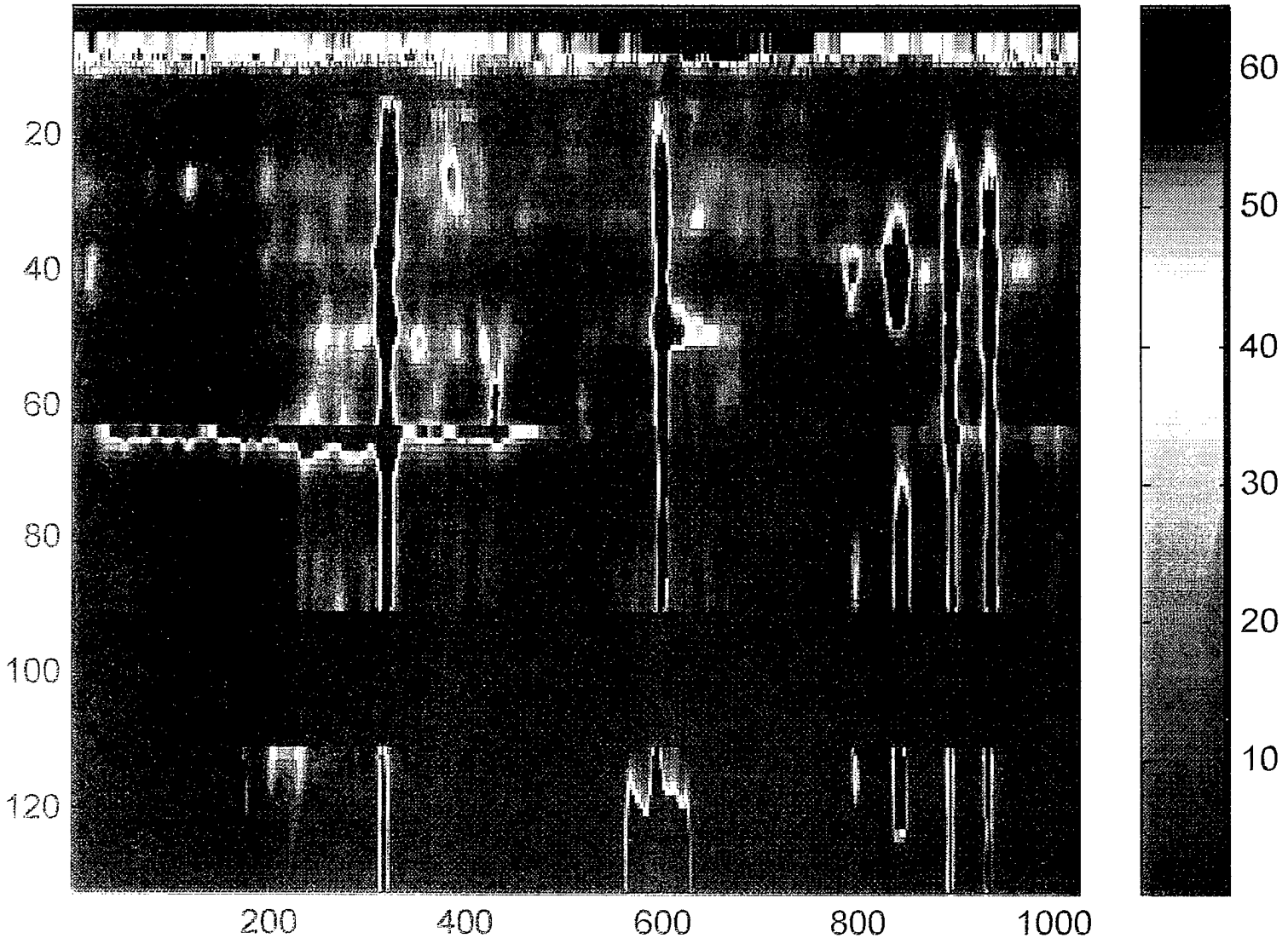


Figure 3.14: Composite scan showing sidewall, shoulder, and crown regions.

connecting scan between the shoulder region and the crown. To compensate, a dead band was inserted in the image between the shoulder and crown inspection regions so simulated flaws would appear in their correct orientation.

The one-half scan demonstrates proof of the inspection concept. The aspect ratio is skewed due to the 1024 length of the scan plotted next to the 120 width. Objects appear to be foreshortened unnaturally. In Figure 3.14 the simulated flaws shown in Figure 3.13 are readily apparent. At the far right in the image are two vertical stripes corresponding to the two foam tapes on the tire. Following the stripes are the large and small squares of foam tape. To the left of the squares is the next stripe shown in Figure 3.13 with a large square blob near the bottom of the image. Inspection of the tire after producing the image showed the blob to be a balance patch glued on the inside of the tire. The final stripe further to the left is the masking tape placed on tire as a low attenuation simulation. Low attenuation at the top of the image is due to the bead in the tire where inspection by ultrasound is not possible. Careful measurement shows that inspection begins as soon as the ultrasound beam is below the bead region.

Figure 3.14 showed an image enhanced to highlight the lowest attenuation locations. The flawed regions are represented by high values due to the inverse scaling applied by the enhancement. Figure 3.15 shows the original data enhanced only by mapping the image onto a 0-80 grayscale. The advantage of the previous method is that highly attenuating areas are easily shown. However, some detail may be lost. Figure 3.15 shows greater detail in the image but needs more interpretation to determine the meaning of low attenuation areas.

In Figure 3.15, the same features as Figure 3.14 are evident but lesser features are also available for review. In particular, sidewall plies become visible including a long thread of low attenuation traveling from the top of the far left stripe to the bottom of the middle stripe. This can be interpreted as failure in the ply along that line.

## 4. Discussion

### 4.1 Point testing

The result of the point test study show that the ultrasonic signal can be detected through the aircraft tire even in the complex region near the bead. This result is critical for demonstrating that tire inspection can be performed using ultrasound in through transmission. In the point test study, it is apparent that the 0.5 MHz frequency suffers fewer losses in the elastic medium, as expected. This is evident from the larger gains that need to be applied to the 2.25 MHz signal for similar received amplitudes.

The 2.25 MHz signal at the bead requires a large degree of amplification with accompanying reduction in signal-to-noise ratio. However, the signal is still easily detected in the noise and attenuation of the signal relative to that of other points in the local area will still be discernable.

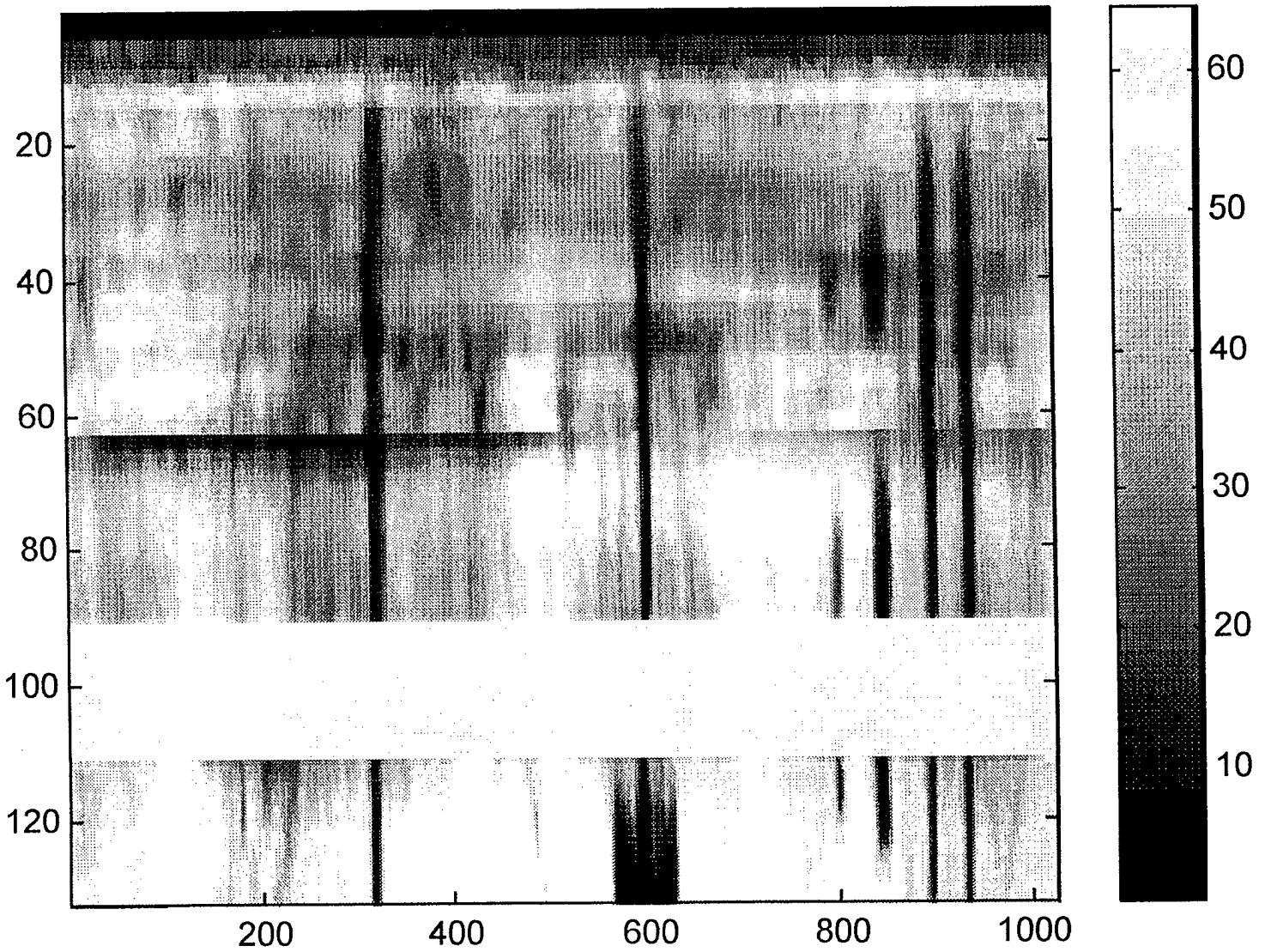

Figure 3.15: Composite scan, minimal processing.

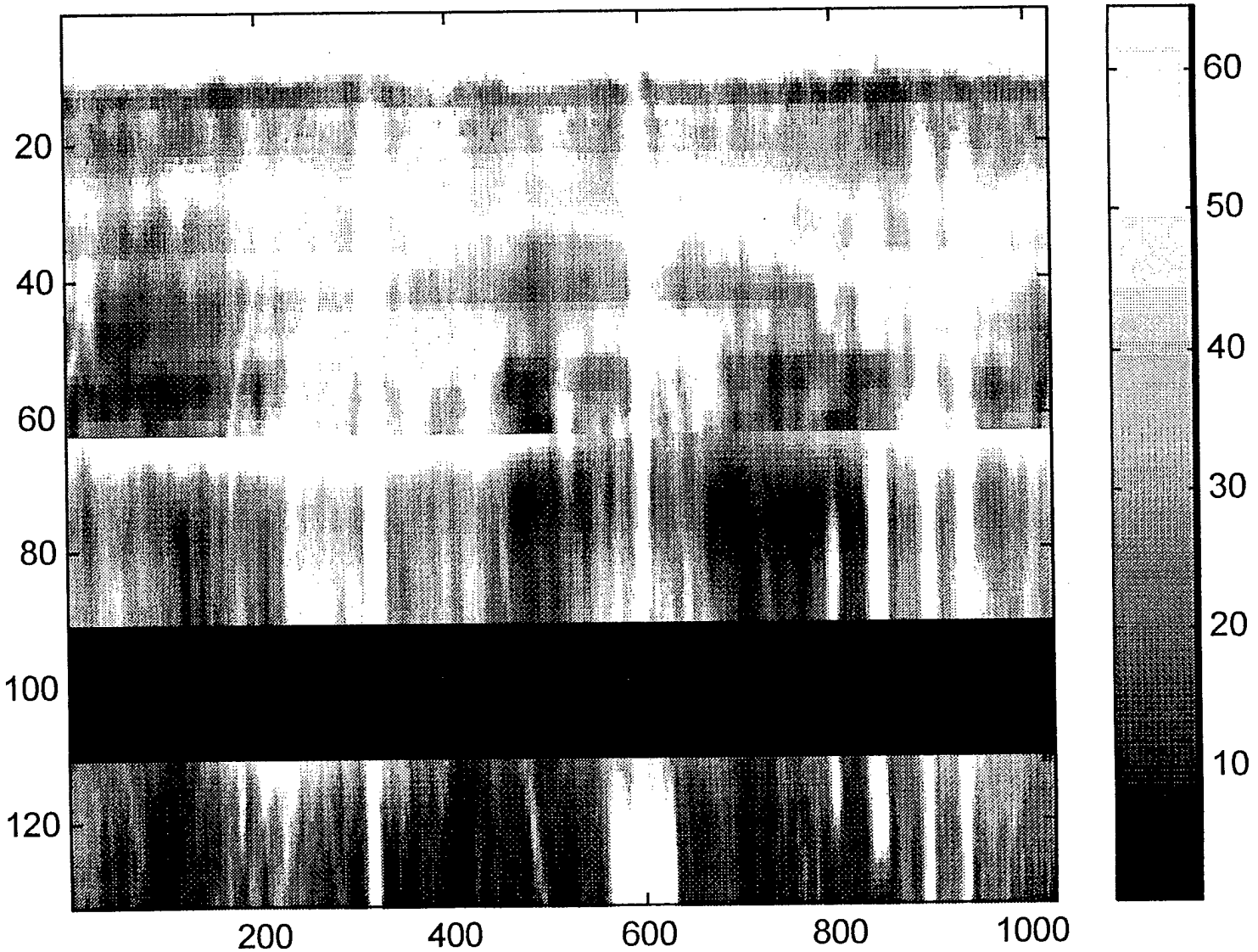

Figure 3.15: Composite scan, minimal processing.

## 4.2 XY scanning

To show the results of point testing are valid, actual scans were performed with simulated flaws. In every case the flaws were detectable with 2.25 MHz ultrasound. The 0.5 MHz does not highlight the detail nearly as well as the 2.25 MHz due to the much larger spot size. In scanning without simulated flaws on the tire section, details of the belt package in the tire sidewall are easily discernable.

One problem with the XY scanning is the constant gain applied over the entire scan. The relatively transparent sidewall does not require as high a gain to be applied to the receiving transducer output as near the bead. For the scans presented here, an average gain was applied that prevented clipping in the amplifiers. However, some form of automatic gain control will enhance the features discernable using 2.25 MHz ultrasound.

## 4.3 Circumferential scanning.

Results from circumferential scanning show great detail is available by ultrasound inspection. In particular, simulated flaws as small as ½" (from the ½" foam tape squares) are easily discernable. Figure 4.1 shows a close-up of one ½" square flaw. The step size

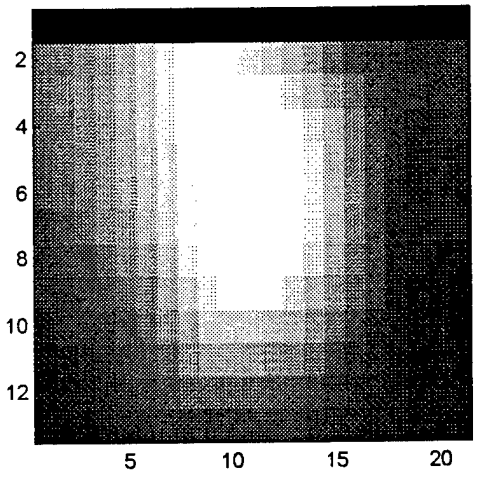


**Figure 4.1: Close-up, 1/2" flaw.**

is 1/16" and the flaw appears as a pixel array of approximately 6-7 pixels square in the central region (as expected for a ½" flaw with 1/16" step size). The point spread function of the transducer contributes to the blurring of the edges. Deconvolution of the point spread function would further enhance the region so the flaw would appear in proper perspective [Dow96].

In addition to the simulated flaws, actual ply failure appears to have been detected in the tire as shown in Figure 3.13. The region is only several pixels wide indicating flaw detection of 1/8" or less is possible.

Examination of the composite shown in Figure 3.13 provides a means to detect flaws that cover large regions of the tire. The flawed ply region detected by examining the large composite region may not have been detectable by examination of a small local region. The flaw is narrow in one direction but is very long as it crosses the tire. This information is available only in a full tire scanning method. In particular, damage of this nature may not be available at all by methods other than ultrasound.

The data can be mapped onto a virtual tire as shown in Figure 4.2 for a more intuitive display of the information. Figure 4.3 shows a grayscale image of the un-enhanced image from Figure 3.15. In these Figures, the detected flaws appear in proper location and perspective and should be compared with the photograph shown in Figure 3.13.

## 5. Future work.

This study has shown that tire inspection is possible for aircraft tires. In this study, only used aircraft tires where inspected. New aircraft tires should also be studied as a basis for comparison with these results. Particularly with regard to the conclusion presented for Figure 3.13 that there is a ply failure indicated by the long diagonal line.

Studying new and used aircraft tires for comparison is a time consuming process without a high-speed, high-resolution scanner developed to inspect the tires. Setup to perform a scan such as that shown in Figure 3.13 required approximately 4 days. Performing the scan itself using equipment modified from a truck tire scanner took approximately 4 hours. Combination and analysis of the resultant scans required several more days. In general, at this point, inspecting a single tire is a several day process. This could be expedited by development of a scanning system. Five minute scans should be possible.

Non-destructive evaluation of materials is an evolving art and the use of ultrasound to inspect aircraft tires with its results is not well understood at this time. A statistical approach would seem appropriate where tires are inspected by ultrasound, gross defects can be rejected but marginal defects may be returned to service for later examination at the next retreading cycle. A continual record of tire wear can be developed with a tire flaw map produced at each cycle. In this way, tire flaws can be characterized and tire may eventually be used indefinitely until wear signs are evident.

## 6. Conclusion

This study has presented a theoretical basis for the operation of transducers used for tire sidewall inspection. Transducers were selected and used to perform a-scans on several

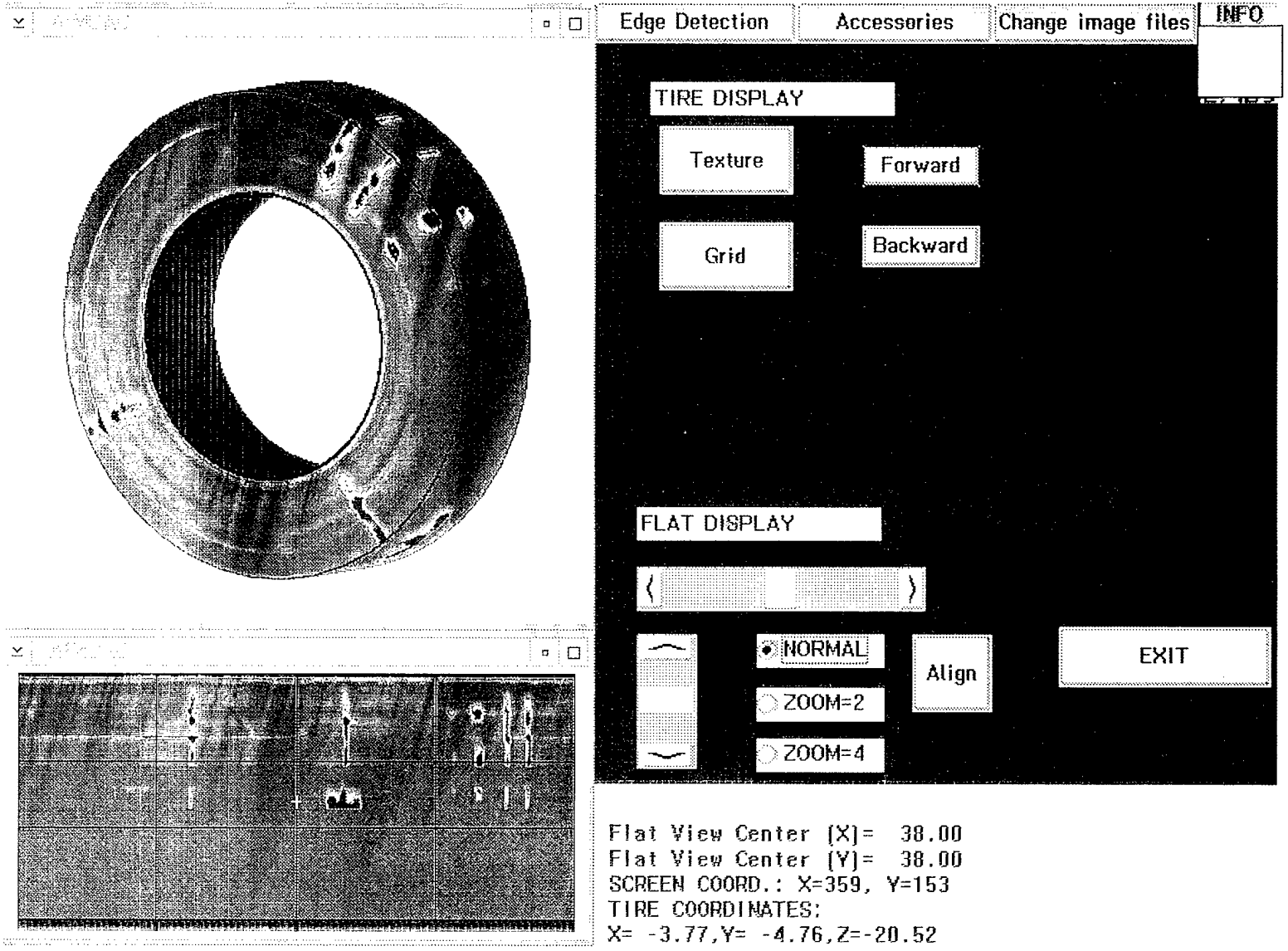


Figure 4.2: Data mapped onto virtual tire.

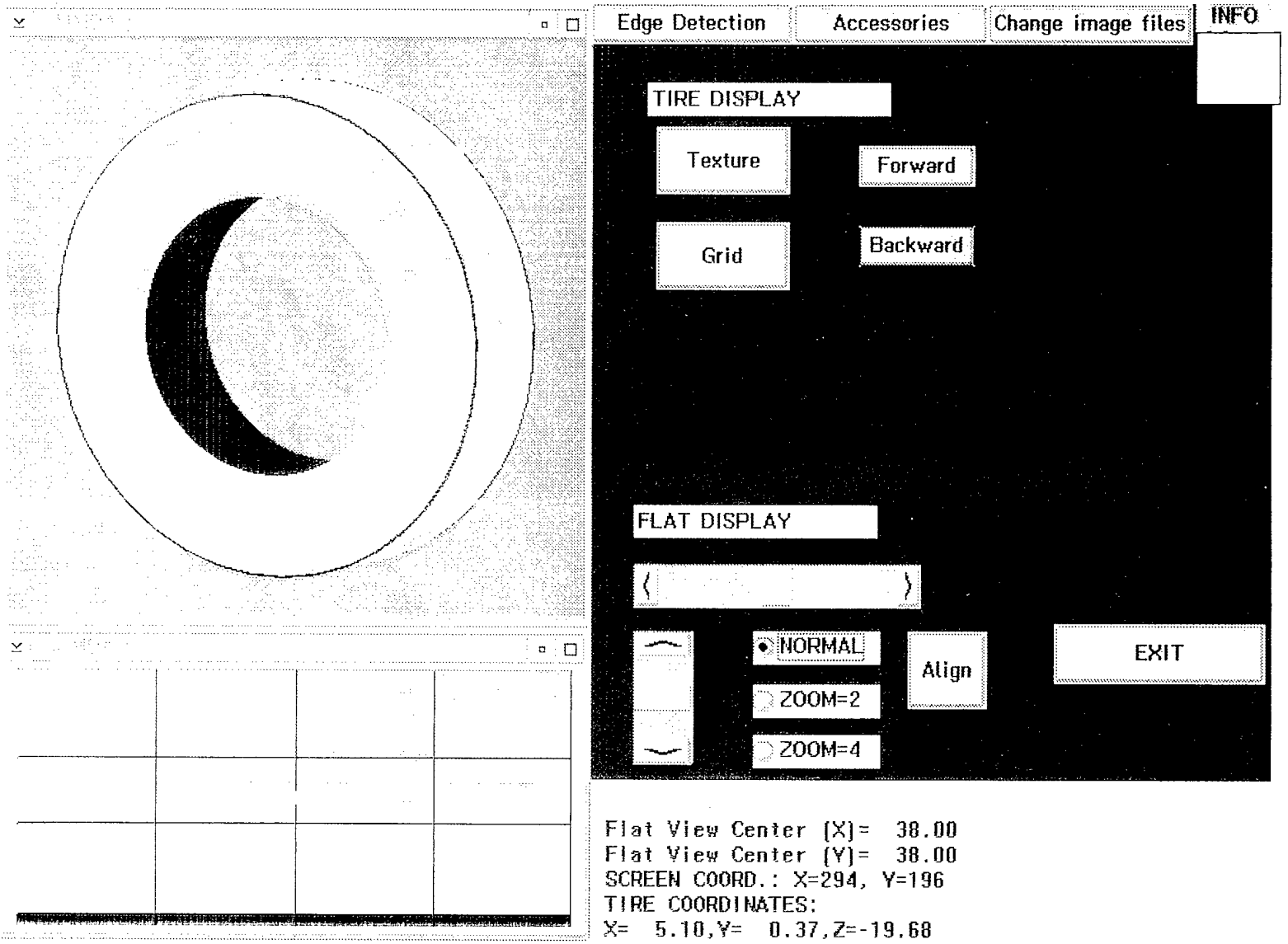


Figure 4.3: Data mapped onto virtual tire.

locations on a tire sidewall to determine if the tire could be inspected over the entire surface. Point testing showed that ultrasound signal would penetrate the sidewall everyplace except the bead region with a measurable output on the opposite side.

XY scans were performed over the surface of a tire section with foam tape attenuation attached to simulate tire flaws. The results of XY scanning show 2.25 MHz ultrasound to be capable of detecting fine flaws by measuring attenuation properties over the surface.

Circumferential scanning showed that full tire scans are possible with easy detection of attenuation property changes. In addition, full tire scans provide greater insight into the nature of tire flaws by imaging the entire tire for inspection instead of regions.

Through transmission ultrasonic inspection where the attenuation properties of the material are measured is shown to be a viable method to inspect aircraft tire sidewalls non-destructively for simulated flaws. Complete tire scans may be made by further development of a scanning system.

## References


[Dow97] Downs, J., *Systems Design of a High-Resolution, Large-Data Set Ultrasonic Tire Inspection Machine*, Doctoral dissertation, Colorado State University, 1997.

[Dow96] Downs, J., Peterson, M.L., *Theoretical, Simulated and Experimental 2-D Resolution Enhancement of an Ultrasonic Transducer by Deconvolution of the Point Spread Function*, Review of Progress in Quantitative Non-Destructive Evaluation, Plenum Press, 1996.

[Fre89] French, Tom, *Tyre Technology*, Adam Hilger, Bristol, 1989.

[Kra83] Krautkramer J., Krautkramer, H., *Ultrasonic testing of Materials*, Springer-Verlag, New York, 1983.

[Pan95] Panametrics, Inc., *Ultrasonic Transducers for Nondestructive Testing*, Product literature by Panametrics, Waltham, MA, 1995.

[Rei97] Reis, H., *Prototype Instrument for Damage Evaluation in Steel Belted Radial Tires Using Acousto-Ultrasonics*, Eigth International Symposium on Non-destructive Characterization of Materials, Boulder, CO, 1997.

[Rog92] Rogers, R., Peterson, M., Achenbach, J.D., *Ultrasonic Testing of Truck Tires Phase II*, Progress Report to Bandag Tire Company, Center for Quality Engineering and Failure Prevention, Northwestern University, Evanston, IL, 1992.